



A semi-analytical temperature solution for multi-segment deep coaxial borehole heat exchangers

Magnus Wangen

Received: 22 August 2022 / Accepted: 12 December 2023
© The Author(s) 2024

Abstract A semi-analytical and a finite-difference scheme are presented for the simulation of temperature and the heat transfer in a multi-segment coaxial borehole heat exchanger. The single-segment solution on closed-form is extended to a semi-analytical multi-segment solution, where each segment may have unique properties. These properties are such as different casings, widths of the annulus, radius of the inner tubing, material properties, rock properties and geothermal gradients. The multi-segment model is a simple and powerful alternative to numerical methods for simulating a complex coaxial borehole heat exchanger with a constant flow rate. It is demonstrated with a deep coaxial borehole heat exchanger made of three different segments. The analytical and semi-analytical models are validated by comparison with numerical solutions obtained with an upstream finite difference scheme. The match between the solutions is excellent. The solution on a closed-form is used to study the temperature difference between the outlet and the inlet regarding two dimensionless numbers. It is found that the maximum temperature difference occurs when the dimensionless heat transfer coefficient for the casing-rock is much larger than one. A second necessary condition is that the dimensionless heat transfer coefficient for the insulator

between the inner tube and the annulus must be much less than one. The power leakage from the inner tubing to the annulus is also at a maximum under these conditions.

Keywords Deep coaxial borehole heat exchangers · Multiple segments heat exchangers · Analytical solution · Dimensionless numbers

1 Article Highlights

- Analytical and numerical solutions for deep borehole heat exchanger
- Semi-analytical solution for multi-segment deep borehole heat exchanger
- Conditions for the maximum temperature difference between the inlet and the outlet.

2 Introduction

Energy production from fossil fuels is responsible for enormous CO₂ emissions. More than 30 Gt of anthropogenic CO₂ has been emitted globally every year since 2000 (International Energy Agency 2016). The rapid increase in atmospheric CO₂ concentrations over the last 100 years is the likely reason for current climate changes (Bryant 1997). The need for alternatives to fossil fuels has resulted in a broad interest

M. Wangen (✉)
Institute for Energy Technology, Instituttveien 18,
Kjeller 2027, Viken, Norway
e-mail: Magnus.Wangen@ife.no

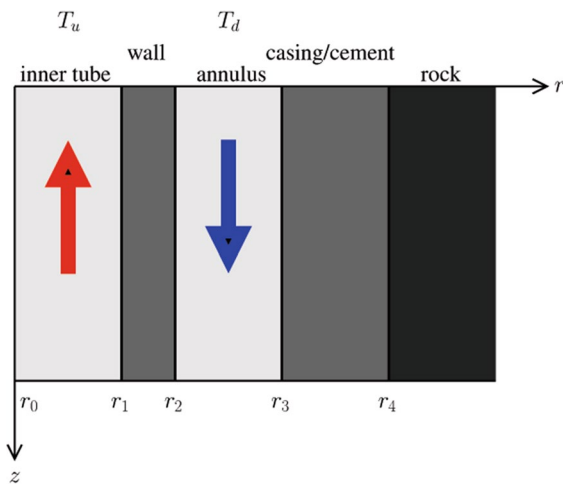


Fig. 1 The well consists of an inner tube separated from an annulus by a wall, and there is a casing between the well and the rock

in geothermal energy. In general, geothermal energy produces little or no CO_2 emissions and requires little surface area (Gehlin et al. 2016). Shallow borehole heat exchangers are widely used for heating and cooling buildings when they are coupled with heat pumps (Sanner et al. 2003).

Shallow borehole heat exchangers normally have a U-tube design. The fluid is heated in one tube going down the well, and the heated fluid returns to the surface through another tube, which is thermally insulated from its surroundings (Gehlin et al. 2016). An alternative to the U-tube is the coaxial borehole heat exchanger (CBHE). A CBHE has a tube-in-tube construction as shown in Fig. 1. The fluid enters the annulus at the top of the well and it is heated from the surrounding rock on its way down. Assuming that the rock temperature increases with depth, the fluid is maximally heated at the base of the well. The fluid returns to the surface through the inner tube, which is insulated from the annulus to avoid heat leakage between the two streams. For shallow geothermal energy, the CBHE has been found to be more efficient than the traditional U-tube (Quaggiotto et al. 2019).

The successful application of shallow borehole heat exchanger (BHE) has given rise to increased interest for deep BHE, and in particular in deep CBHE (DCBHE). Deep geothermal energy is defined by Breede et al. (2015) to be a depth of at least 400 m

and a temperature of at least 20°C . Although other authors recommend depths of at least 1000 m and temperatures of more than 60°C (Breede et al. 2015). The term medium-deep has been applied to wells with depths from several hundred meters to 3000 m, where the rock temperature is between 70°C and 90°C (Ma et al. 2020). This temperature range is not suitable for electricity production, but it is well suited for district heating in cold areas with long heating seasons. Two-phase flow in the DBHE may be a challenge when circulating water is heated to more than 100°C . In the following, it is assumed that the fluid is always in the liquid phase.

Modelling BHE can be divided into two groups: analytical and semi-analytical models and numerical models. The analytical models are normally made in the cylinder coordinates assuming cylinder symmetry around a vertical well. These models provide much insight into coaxial borehole systems, and they often have a low computational cost. An important temperature solution for heat flow problems in solids is the infinite point source solution (Carslaw and Jeager 1959). It is the basis for the infinite line source model (Carslaw and Jeager 1959), which is often used for heat flow towards a well. There are much fewer analytical models for deep geothermal energy than for shallow. For shallow BHE, there are several models for the transient energy production or energy storage that build on the pioneering work of Ingersoll (Ingersoll et al. 1954) for heat conduction in solids (Beier et al. 2013; Li and Lai 2015; Zhang et al. 2016; Bandos et al. 2009). Several of these models deal with thermal response testing (TRT), where the inlet and the outlet temperatures are measured when heat at a constant power is delivered to the borehole. Calibrating the inlet and outlet temperatures with a linear heat source model yields average values of thermal conductivity, thermal borehole resistance and ground temperature (Witte 2007).

In the rock, heat convection may dominate heat conduction in the case of groundwater flow. Two early analytical models to deal with heat convection in addition to conduction were introduced by Sutton et al. (2003), Diao et al. (2004) based on the moving line source model from (Carslaw and Jeager 1959). These two models assume a constant Darcy flux in the plane normal to the well. The thermal impact of more complicated flow regimes on a geothermal well needs

numerical treatment. It should be mentioned that the moving line source solution of the convection-diffusion equation has applications in various fields such as the measurement of groundwater flow (Simon et al. 2021) and the distribution of contaminants in the groundwater (Antelmi et al. 2020).

The numerical models can be subdivided into those based on cylinder symmetry and those that are in full 3-D. 3-D models can account for the full geometry when the cylinder symmetry is not valid. This may be the case for the U-tube BHE. For example, a 3-D model for DCBHE has been developed (Gascuel et al. 2022), which is based on the FEFLOW numerical library (Diersch 2013). Numerical models have an advantage over analytical models in that they are flexible with respect to the operating conditions such as flow rates, injection temperatures, rock properties, geothermal gradients, different casings and cement thickness. The numerical models can also be extended more easily than the analytical ones to greater depths. Cylinder symmetrical models are made with finite difference schemes (Shao et al. 2016) or with software such as COMSOL-multiphysics (Zanchini et al. 2010). Shao and coauthors (Shao et al. 2016) explained in detail how a numerical model for a BHE is built using the finite difference method.

So far, only a few DBHE have been tested in real life, and knowledge of DBHE is largely based on modelling (Kohl et al. 2002; Beier 2020; Ma et al. 2020; Gascuel et al. 2022). An abandoned 2300 m deep borehole in Switzerland has been used to generate geothermal energy (Kohl et al. 2002). In this case, simulations showed that the heat production from the well could be increased to over 200 kW, which is more power per meter well than for a shallow BHE. (Gascuel et al. 2022) have carried out a detailed design study of DCBHE that accounted for different drilling options, materials used, and operating conditions, and they estimated a price per kW for different alternatives.

Kabir et al. (1996), Tóth and Bobok (2008), Tóth and Bobok (2016), Sharma et al. (2020) have presented highly useful analytical models for a DCBHE. An analytical solution of CBHE was provided by (Kabir et al. 1996) in the context of well-control operation. The model (Kabir et al. 1996) can answer several questions related to the design of a DCBHE,

such as well depth and flow rate. It assumes a constant flow rate, cylinder symmetry around the well and a model for the heat flow towards a well from the surrounding rock, for instance, such as Ramey's approximation (Ramey 1962). Ramey's approximation has an initial rock temperature that increases linearly with depth.

The model proposed in this article builds on the works of Kabir et al. (1996), Tóth and Bobok (2008), Tóth and Bobok (2016), Al Saedi et al. (2018), Al Saedi et al. (2019), Sharma et al. (2020). A solution of their model is obtained by a different approach which keeps the first-order nature of the problem. Then, the solution is expressed in terms of eigenvectors and eigenvalues of the main matrix of the model (Kreyszig 2020). This alternative approach has only two linearly independent undetermined coefficients, which are obtained using two boundary conditions. The result is a simple solution on closed-form that allows for a straightforward generalization to a DCBHE with multiple segments. Sharma et al. (2020) presents a similar two-segment model for the simulation of a horizontal geothermal well. Each segment may have its own properties, such as casing, the width of the annulus, the radius of the inner tubing, material properties, rock properties and the geothermal gradient. There are two unknown coefficients in the temperature solution for each segment, and they are obtained from the requirement that the temperature is continuous at each interface between segments. The fluid has the same temperature at the outlet of one section as at the inlet of the following section. The coefficients for a multi-segment well are obtained by solving a small linear equation system, where there are two unknown coefficients per segment. For instance, a 3-segment model gives a linear equation system for 6 unknown coefficients. This model does not account for heat convection by groundwater flow because it is not yet clear if Ramey's approximate solution can be extended to include heat convection.

The manuscript is organized as follows: The equations of the model and the solution are discussed first. The difference in output and input temperatures is then discussed in terms of dimensionless numbers. The multi-segment solution is presented and tested. Finally, there is an example of a temperature solution for DCBHE made of three different segments.

3 The equation for the vertical coaxial borehole heat exchanger

The following two equations give the temperature of the fluid in a coaxial borehole heat exchanger assuming cylinder symmetry

$$\frac{dT_d}{dz} = K_w(T_u - T_d) + K_r(t)(T_r - T_d) \tag{1}$$

$$\frac{dT_u}{dz} = K_w(T_u - T_d), \tag{2}$$

where T_d is the temperature of the fluid flowing down the annulus, T_u is the temperature of fluid flowing up the inner tube, and T_r is the initial rock temperature (Tóth and Bobok 2008, 2016). The z -coordinate points downwards, where $z = 0$ is the surface, and t is the time. The first term on the right-hand side of Eq. (1) represents heat flow from the inner tube to the annulus, and the second term is the heat flow from the rock to the annulus. Appendix A shows how Eqs. (1) and (2) follow from energy conservation in the annulus and the inner tube. The coefficient K_w is the overall heat transfer coefficient U_w between the inner tube and the annulus,

$$K_w = \frac{U_w dA_w/dz}{C_f \dot{m}}, \tag{3}$$

where C_f is the heat capacity of the fluid, \dot{m} is the fluid flow rate as mass per time, and dA/dz is the surface area per length of the wall between the inner tube and the annulus. Notice that the two factors U_w and dA/dz do not appear separately, but only as a product. The overall heat transfer coefficient for the wall is

$$\frac{1}{U_w dA_w/dz} = \frac{1}{2\pi r_1 U_1} + \frac{\ln(r_2/r_1)}{2\pi \lambda_w} + \frac{1}{2\pi r_2 U_2} \tag{4}$$

where U_1 is the heat transfer coefficient between the inner tube and the tube wall, and U_2 is the heat transfer coefficient between the other side of the tube wall and the annulus (Incorpera et al. 2011). The tube wall is between the two radii, r_1 and r_2 , as shown in Fig. 1, and its heat conductivity is λ_w . The Nusselt numbers for the inner tube and the annulus give the heat transfer coefficients U_1 and U_2 , respectively. The following simulations use the Nusselt number (Incorpera et al. 2011)

$$Nu = \begin{cases} 0.027 Re^{4/5} Pr^{0.33} & \text{for } Re > 10^4 \\ 3.66 & \text{for } Re < 10^4 \end{cases} \tag{5}$$

where Re and Pr are the Reynolds number and the Prandtl number, respectively. The coefficient

$$K_r(t) = \frac{2\pi r_3 U_r(t)}{C_f \dot{m}}, \tag{6}$$

controls the heat transfer from the rock towards the well, and it follows from a time-dependent heat transfer coefficient $U_r(t)$. The coefficient $U_r(t)$ accounts for the cooling of the rock. It can also be expressed as the sum of three thermal resistivities as

$$\frac{1}{U_r(t)} = \frac{1}{U_3} + \frac{r_3 \ln(r_4/r_3)}{\lambda_c} + \frac{r_3 f(t)}{\lambda_r} \tag{7}$$

where U_3 is the heat transfer coefficient between the fluid and the outer wall of the annulus. The λ_c is the average heat conductivity between the radii r_3 and r_4 , which is the material that separates the annulus from the rock. This material could represent a steel casing and the cement between the casing and the rock. The third term in Eq. (7) is the time-dependent thermal resistance of the rock. It is based on an approximation introduced by Ramey (Ramey 1962) for the heat flow towards a well. Ramey (Ramey 1962) showed that the heat flow radially towards a well in the interval dz can be approximated as

$$dq = \frac{2\pi \lambda_r (T_4 - T_r) dz}{f(t)} \tag{8}$$

where λ_r is the heat conductivity of the rock, T_4 is the temperature at radius r_4 (see Fig. 1), and

$$T_r(z) = az + b \tag{9}$$

is the initial rock temperature. The temperature of the rock increases linearly with depth, having a geothermal gradient a , and a surface temperature b . Both the temperature T_4 and the heat flow dq depend on time, and an exact expression for the ratio turns out to be a non-trivial problem. As demonstrated by Ramey (Ramey 1962), the time dependence can be approximated as

$$f(t) = -\ln\left(\frac{r_3}{2\sqrt{\alpha t}}\right) - 0.288 \tag{10}$$

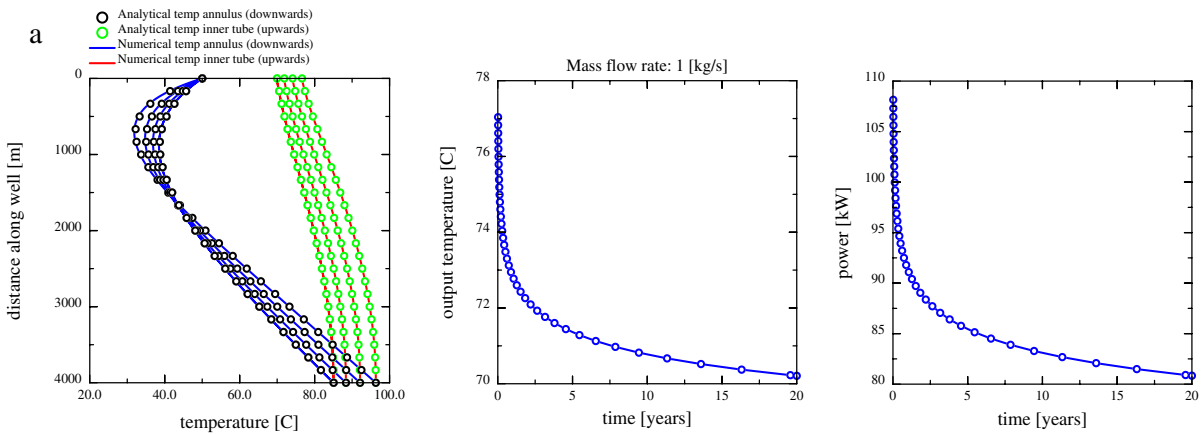


Fig. 2 a The well temperature at 10 days, 100 days, 1000 days and 10,000 days. b The output temperature as a function of time. c The output power as a function of time

where α is the heat conductance of the rock. Ramey (Ramey 1962) demonstrated that the approximation (8) gets better with increasing time. The use of expression $f(t)$ gives quite accurate results after only one day and very good results after one week (Ramey 1962). The increasing accuracy of the Ramey solution with increasing time makes it useful

Table 1 Fluid properties

| | |
|--|-------|
| c_f (fluid heat cap) [J kg ⁻¹ K ⁻¹] | 4000 |
| λ_f (fluid heat cond) [W m ⁻¹ K ⁻¹] | 0.6 |
| ρ_f (fluid density) [kg m ⁻³] | 1000 |
| μ (fluid viscosity) [Pa s] | 0.001 |

Table 2 Input data for multi-segment test case

| | |
|---|---------------------|
| Segment number [-] | 0 |
| L (length) [m] | $4.0 \cdot 10^3$ |
| r_1 (radius inner tube) [m] | $1.0 \cdot 10^{-1}$ |
| d_w (thickness wall) [m] | $2.0 \cdot 10^{-2}$ |
| d_a (thickness annulus) [m] | $5.0 \cdot 10^{-2}$ |
| d_c (thickness casing) [m] | $5.0 \cdot 10^{-2}$ |
| λ_w (wall heat cond) [W m ⁻¹ K ⁻¹] | $1.0 \cdot 10^{-3}$ |
| λ_c (casing heat cond) [W m ⁻¹ K ⁻¹] | 3.50 |
| c_r (rock heat cap) [J kg ⁻¹ K ⁻¹] | $1.0 \cdot 10^3$ |
| λ_r (rock heat cond) [W m ⁻¹ K ⁻¹] | 3.50 |
| ρ_r (rock density) [kg m ⁻³] | $2.25 \cdot 10^3$ |

for benchmarking numerical codes simulating geothermal wells over several years. For instance, Gola et al. (2022) compare their numerical results with Ramey solutions and the match is excellent.

The full solution of Eqs. (1) and (2) is given in Appendix B by Eqs. (21) to (29). In addition to the two coefficients K_w and K_r , the solution depends on the inlet temperature T_0 , the well length L , and the initial rock temperature by the parameters a and b . Appendix C shows that the full solution of Appendix B reproduces Ramey’s solution in the limit where $K_w \rightarrow 0$. It should also be mentioned that Eqs. (1) and (2) reduce to the equations for a standard counter flow heat exchanger when $K_r = 0$, (Incorpera et al. 2011).

4 The temperature solution

Figure 2 shows an example of the temperature solution for $T_d(z)$ and $T_u(z)$ of the two coupled Eqs. (1) and (2). The temperature is computed using expression (21) from Appendix B. The fluid has properties of water (see Table 1), and Table 2 lists the case data. The rock heat conductivity is $\lambda_r = 3.5 \text{ W m}^{-1} \text{ K}^{-1}$ and the heat conductivity of the insulator between the inner tube and the annulus is $\lambda_w = 1 \cdot 10^{-3} \text{ W m}^{-1} \text{ K}^{-1}$. The mass flow rate is 1 kg s^{-1} . In Fig. 2a, the temperature in the annulus is blue, and the temperature in the return tube is red. The temperatures are plotted at 10 days, 100 days,

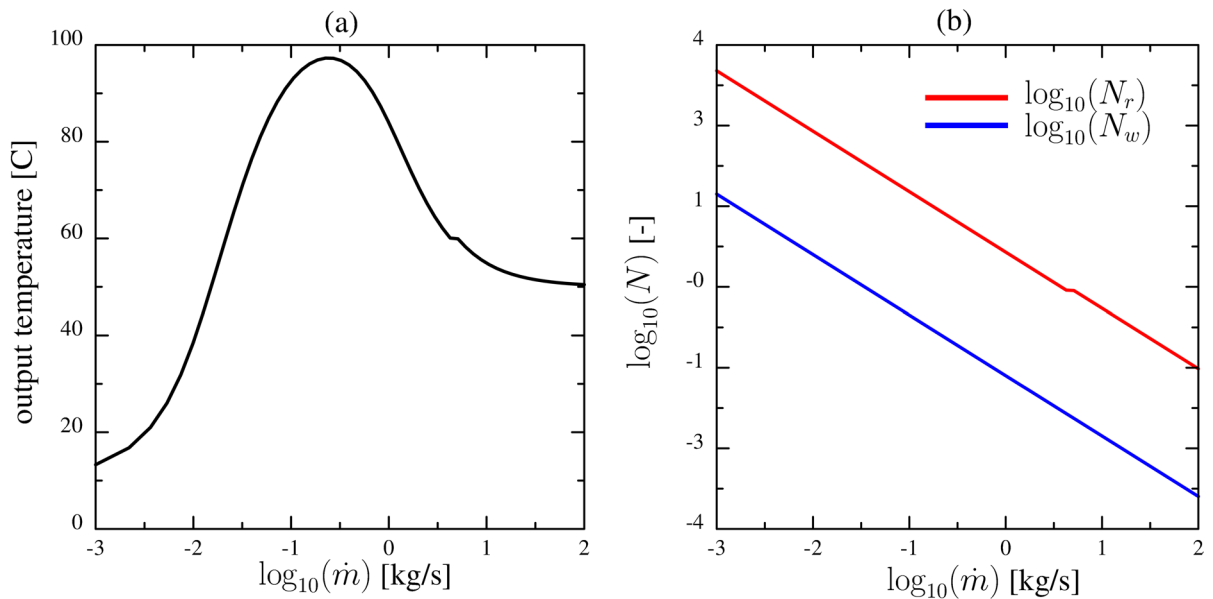


Fig. 3 **a** The outlet temperature for different flow rates at 5 years. **b** The dimensionless numbers N_r and N_w for the same rates as in **a**

1000 days (2.7 years) and 10,000 days (27.3 years). The well is 4 km deep, and the initial rock temperature increases from a constant surface temperature of 10 °C to a temperature of 110 °C at the depth of the well, which makes the geothermal gradient 25 °C/km. The solution is demonstrated with an injection temperature of 50 °C, which leads to the heating of the rock surrounding the upper part of the well. The moderate mass flow rate slowly cools the lower part of the well with time. The slow cooling is also observed from the output temperature plotted as a function of time in Fig. 2b. The output temperature decreases from 95 °C to 80 °C over 27 years. The power, plotted in Fig. 2c, follows the output temperature because the output power is proportional to the difference in temperature between the outlet and the inlet (see Appendix B). The analytical solution in Fig. 2a is verified by comparison with a numerical finite difference solution. The match is excellent. Appendix E provides details of the finite difference method used.

5 Dimensionless numbers

The behaviour of a CBHE can be understood in terms of two dimensionless numbers:

$$N_r = K_r L \quad \text{and} \quad N_w = K_w L \quad (11)$$

Several authors have used these dimensionless numbers to analyse CBHEs (Beier 2011; Beier et al. 2014; Luo et al. 2019). Beier (Beier 2011) expressed the error in the total thermal resistance using N_r and N_w . These numbers are also useful in the study of the outlet temperature for different mass flow rates. Figure 3a shows the outlet temperature as a function of the mass flow rate. A “low” mass flow rate gives a fluid temperature nearly the same as the temperature of the surrounding rock. In the other regime with a “high” mass flow rate, the output temperature is nearly the same as the input temperature. Intermediate flow rates produce a noticeable difference between the initial rock temperature and the inlet temperature. Figure 3b shows N_r and N_w as functions of the mass flow rate. The outlet temperature is at a maximum when $N_r \gg 1$ and $N_w \ll 1$. These two conditions define an intermediate flow rate. The first inequality can be interpreted as a condition for when the surrounding rock provides heat to the fluid in the annulus. The inequality $N_w \ll 1$ is a condition for when the inner tubing is a good insulator.

The dimensionless numbers can be interpreted as ratios of powers. For instance, N_w can be written

as $N_w = P_w/P_f$, where $P_w = U_w(dA_w/dz)L\Delta T$ and $P_f = C_f\dot{m}\Delta T$. The power P_w is the leakage from the inner tube to the annulus by a temperature difference ΔT , and the power P_f is the additional power carried by the fluid when the temperature increases with ΔT .

6 Multi-segment solution

In the case of one segment, the solution for the fluid temperature in the annulus and the inner tube is given by Eqs. (21) and (22) in Appendix B. These two equations have two unknown coefficients, D_1 and D_2 . In the case of just one well segment, these two constants are determined by the knowledge of the injection temperature, $T_d(z=0) = T_0$, and the fact that the temperature at the base of the well is the same in the annulus and the inner tube, $T_d(z=L) = T_u(z=L)$. Appendix B gives the coefficients D_1 and D_2 .

To extend the one-segment model to multiple segments, it is advantageous to introduce the notation E_k and F_k for the two parameters D_1 and D_2 , respectively, for segment number k . According to Appendix D, the temperature in segment k can then be written as

$$T_{d,k}(z) = E_k \cdot e_k(z) + F_k \cdot f_k(z) + p_k(z) \tag{12}$$

$$T_{u,k}(z) = E_k \cdot g_k(z) + F_k \cdot h_k(z) + q_k(z). \tag{13}$$

The z -coordinate is now local in each segment where the top of the segment is at $z = 0$, the base of the segment is at $z = L_k$, and L_k is the length of segment k . The counting of the segments starts from the surface, and the segment numbers increase with depth. The unknown parameters E_k and F_k are found by requiring that the temperature is continuous across each segment interface. At the interface between segment k and $k + 1$, the temperature solution satisfies

$$\begin{aligned} T_{d,k}(z = L_k) &= T_{d,k+1}(z = 0) \quad \text{and} \\ T_{u,k}(z = L_k) &= T_{u,k+1}(z = 0) \end{aligned} \tag{14}$$

In addition to the continuity of the temperature at the interfaces between the segments, the temperature at the inlet of the first segment is given and the temperature at the base of the last segment is the same in the annulus and the inner tube. In the case of N segments, this gives $2N$ linear equations for the $2N$ unknown coefficients E_k and F_k . There does not seem to be a

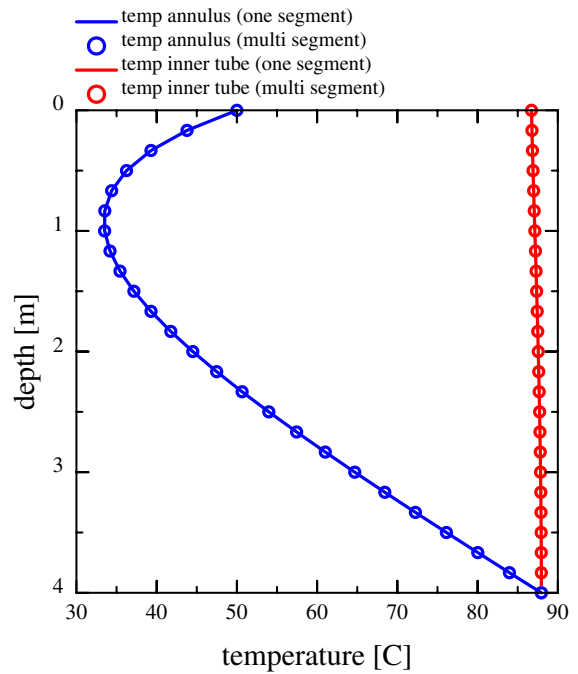


Fig. 4 The well temperatures for a single segment solution and for the same segment dived into 10 segments. The two solutions are the same

simple analytical solution for this linear system of equations, unlike the case of just one segment.

Concerning programming, it is advantageous to represent the segments by a class using an object-oriented language like Python. The multi-segment model is then a list of objects of a class segment. Once the parameters E_k and F_k are known, it is straightforward to compute the temperature in the annulus and the inner tube using the functionality of each object of class segment. The multi-segment model is a semi-analytical alternative to numerical methods for simulating a DBHE. The semi-analytical solutions are well suited to benchmark numerical solutions because they do have discretization errors.

A test of the multi-segment approach is to take a reference segment and split it into an arbitrary number of equally long subsegments. The multi-segment solution should be exactly the same as the one-segment solution in Appendix B. Figure 4 shows the temperature solution of a reference segment and the multi-segment solution when the reference segment is split into 10 equal subsegments. Table 2 gives the

input parameters for the case. The single segment and the multi-segment solutions are exactly the same, as seen from Fig. 4. This demonstration case has an inlet temperature $T_0 = 50\text{ }^\circ\text{C}$ which is considerably higher than the surface temperature. The fluid is therefore cooled by the rock in the upper part of the well until the surrounding rock temperature becomes higher than the fluid temperature. This happens below the depth of approximately 1 km.

7 Example: vertical coaxial well with three different segments

This demonstration case is a 3000 km vertical well with 3 segments of 1000 m. Table 3 lists the input parameters for each segment. It shows that the well radius is decreasing from 31.5 cm for the top segment to 21.5 cm for the base segment. The inner tube is the same for all segments, and it has a radius of $r_1 = 5\text{ cm}$ and a wall thickness of 1.5 cm. The well segments go through rocks with different heat conductivities. The heat conductivity increases with depth. It is $1.5\text{ W m}^{-1}\text{ K}^{-1}$ for the uppermost segment, $2\text{ W m}^{-1}\text{ K}^{-1}$ for the middle segment, and $2.5\text{ W m}^{-1}\text{ K}^{-1}$ for the base segment. The inner tube is a vacuum insulator with a heat conductivity of $\lambda_w = 0.01\text{ W m}^{-1}\text{ K}^{-1}$ and it is the same for all segments (Damour and Johannsson 2016). Leakage of circulation fluid into the surrounding rock is prevented by sealing the well from the rock. The sealing is also the same for all segments, and it has a heat conductivity of $\lambda_c = 3.5\text{ W m}^{-1}\text{ K}^{-1}$.

Derived parameters for each well segment are listed in Table 4 for a mass flow rate of 2 kg s^{-1} . The Reynolds numbers show that the flow regime in the annulus is between laminar and turbulent, while it is turbulent in the inner tube. The reason is that the annulus has a larger cross-section than in the inner tube, so the velocity in the annulus is lower than in the inner tube. Therefore, the Nusselt number is lowest in the annulus.

The low heat conductivity of the vacuum insulator dominates the overall heat transfer coefficient for the insulating wall. Tables 3 and 4 give that $r_1 U_1 = 58.5\text{ W m}^{-1}\text{ K}^{-1}$, $\lambda_w / \log(r_2/r_1) = 0.038\text{ W m}^{-1}\text{ K}^{-1}$ and $r_2 U_2 = 1.43\text{ W m}^{-1}\text{ K}^{-1}$ in the middle segment for a mass flow rate of 2 kg s^{-1} . The λ_w -term control

the denominator of the overall heat transfer coefficient (4). Therefore, the energy leakage through the wall is only weakly dependent on the fluid velocities in this case.

The multi-segment solution gives the well temperature down the annulus and up the inner tube at a given time assuming a constant flow rate. Figure 5 shows the well temperature at 1 day, 10 days, 100 days and 1000 days for the 3 mass flow rates 0.2 kg s^{-1} , 2 kg s^{-1} and 20 kg s^{-1} . The solutions for 1 day may be at the limit of when Ramey's approximation is good. The figure shows the three thermal regimes under which the geothermal well can operate. Figure 5a has a "low" flow rate, and the temperature in the annulus is nearly in thermal equilibrium with the surrounding rock. The initial rock temperature increases linearly from $10\text{ }^\circ\text{C}$ on the surface to $110\text{ }^\circ\text{C}$ at the base of the well. After 1000 days, the temperature in the annulus remains close to the initial rock temperature. The fluid loses temperature as it rises in the inner tubing because of the low circulation rate, and the return temperature is roughly $20\text{ }^\circ\text{C}$ less than the initial rock temperature at the base of the well.

Figure 5c shows the opposite regime of a "large" circulation rate. The circulation temperature is large enough to cool the well to nearly the injection temperature of $15\text{ }^\circ\text{C}$. After 1000 days of operation, the base temperature of the annulus is barely $20\text{ }^\circ\text{C}$. The circulation rate is sufficiently high for the fluid to avoid a noticeable temperature loss as it returns to the surface in the inner tube. Figure 5b shows an intermediate circulation rate where the temperature increase in the annulus is roughly halfway between the injection temperature and the initial rock temperature.

The semi-analytical solutions in Fig. 5 are verified by comparison with numerical finite difference solutions of the Eqs. (1) and (2). The match between the solutions is excellent. Appendix E presents the details of the finite difference scheme used in the numerical computations.

The three regimes of Fig. 5 are seen in Fig. 6a, where the outlet temperature is plotted as a function of the circulation rate after 5 years of heat production when the input temperature is $15\text{ }^\circ\text{C}$. The maximum output temperature is nearly $70\text{ }^\circ\text{C}$ for the rate of 0.4 kg s^{-1} . For rates much less than 0.4 kg s^{-1} the well output temperature is close to the initial rock

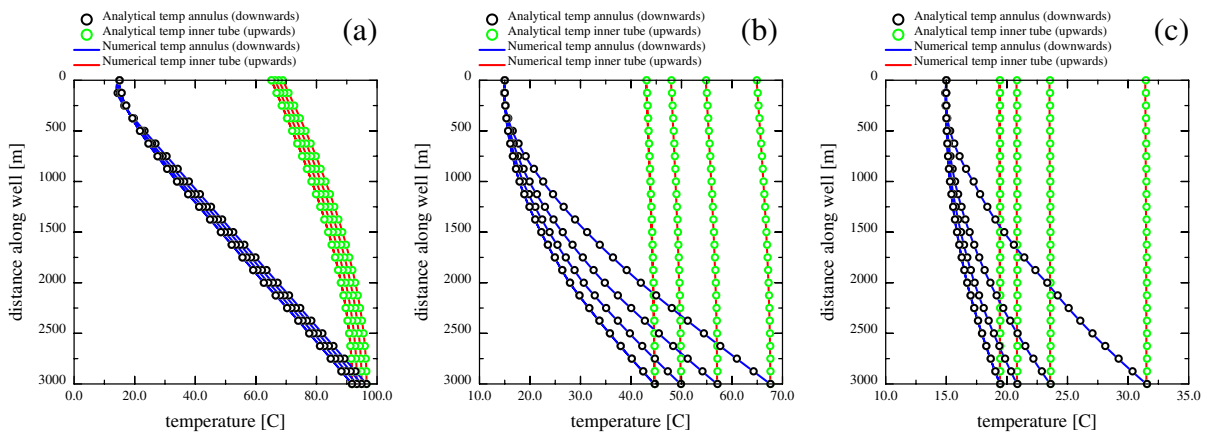


Fig. 5 The well temperature at 1 day, 10 days, 100 days and 1000 days for the 3 mass flow rates 0.2 kg s^{-1} , 2 kg s^{-1} and 20 kg s^{-1}

temperature. On the other hand, very high rates much larger than 0.4 kg s^{-1} give a return temperature close to the injection temperature.

Figure 6b shows that the power increases as a function of increasing flow rate. There is a small kink on the power curve at the rate 4 kg s^{-1} , which is due to the transition from laminar flow to turbulent flow. At this point, the Nusselt number increases from 3.66 at laminar conditions as seen from Eq. (5). The power leakage from the inner tube to the annulus also is shown. The leakage researches a maximum for almost the same flow rate as the maximum output temperature.

The power produced as a function of time is shown in Fig. 7. After a transition lasting a few months, the output power in the example above becomes stable at $\approx 250 \text{ kW}$ for the mass flow rate of 2 kg s^{-1} . The power output is stable for more than 10 years. It can be shown that the output power remains stable for several decades.

8 Conclusion

A semi-analytical model is presented for a multi-segment deep borehole heat exchanger. It builds on the known analytical solution of (Kabir et al. 1996), and it makes use of Ramey’s approximate solution for the heat flow towards a well from the surrounding rock (Ramey 1962). An alternative derivation of the solution is presented, which is based on eigenvalues and eigenvectors. This approach, which preserves the

first order nature of the problem, introduces only two integration constants. The solution is demonstrated with cases showing the cooling of the fluid in the upper part of the annulus before the fluid is heated in the lower part. These examples also show the leakage of heat between the inner tube and the annulus. The analytical solution is discussed in terms of two dimensionless numbers, which are the casing-rock heat transfer coefficient (N_r) and the heat transfer coefficient between the inner tube and the annulus (N_w). It is shown that the maximum temperature difference between the outlet and the inlet of the DCBHE takes place when $N_r \gg 1$ and $N_w \ll 1$. The maximum power leakage from the inner tube to the annulus takes place under the same conditions. The closed-form temperature solution for one segment is extended to a semi-analytical multi-segment solution, where each segment has independent properties of the other segments, such as inner tube radius, annulus thickness, the insulator, casing and rock heat conductivities, and initial rock temperature. The segments are connected by requiring that the temperature is continuous across the segment interfaces. The multi-segment solution is tested by taking a reference segment and dividing it into an arbitrary number of sub-segments. It is demonstrated that the multi-segment temperature solution is the same as for the reference segment. An upstream finite-difference scheme is presented for the temperature solution of the equations of the coaxial borehole heat exchanger. The closed-form solution and the semi-analytical multi-segment solutions are verified by comparing them with the

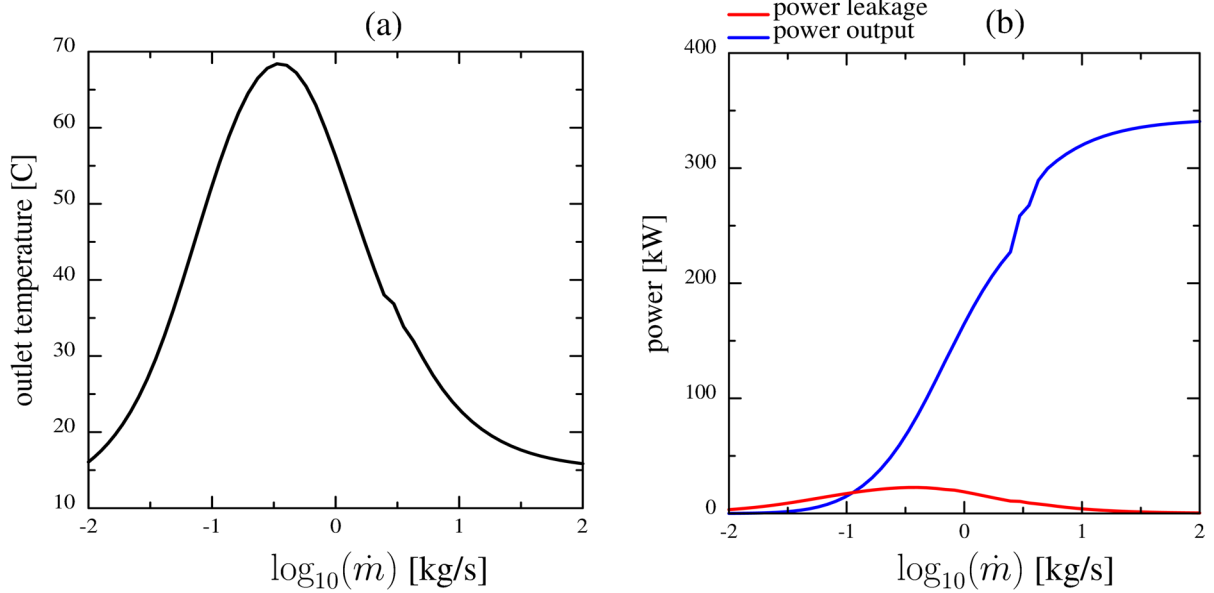


Fig. 6 **a** The output temperature as a function of the mass flow rate. **b** The output power and the power leakage as a function of the mass flow rate

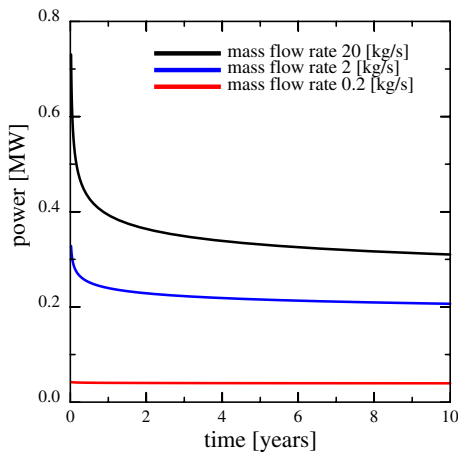


Fig. 7 Power as a function of time for mass flow rates 0.2 kg s^{-1} , 2 kg s^{-1} and 20 kg s^{-1}

numerical finite difference solutions, and the match is excellent. These analytical and semi-analytical solutions are well suited for benchmarking numerical models of borehole heat exchanges, because they do not have discretization errors. They are also

Table 3 Input data

| Segment number [-] | 1 | 2 | 3 |
|--|---------------------|---------------------|---------------------|
| L (length) [m] | $1.0 \cdot 10^3$ | $1.0 \cdot 10^3$ | $1.0 \cdot 10^3$ |
| r_1 (radius inner tube) [m] | $5.0 \cdot 10^{-2}$ | $5.0 \cdot 10^{-2}$ | $5.0 \cdot 10^{-2}$ |
| d_w (thickness wall) [m] | $1.5 \cdot 10^{-2}$ | $1.5 \cdot 10^{-2}$ | $1.5 \cdot 10^{-2}$ |
| d_a (thickness annulus) [m] | 0.15 | $1.0 \cdot 10^{-1}$ | $5.0 \cdot 10^{-2}$ |
| d_c (thickness casing) [m] | $1.0 \cdot 10^{-1}$ | $1.0 \cdot 10^{-1}$ | $1.0 \cdot 10^{-1}$ |
| λ_w (wall heat cond) [$\text{W m}^{-1} \text{K}^{-1}$] | $1.0 \cdot 10^{-2}$ | $1.0 \cdot 10^{-2}$ | $1.0 \cdot 10^{-2}$ |
| λ_c (casing heat cond) [$\text{W m}^{-1} \text{K}^{-1}$] | 3.50 | 3.50 | 3.50 |
| c_r (rock heat cap) [$\text{J kg}^{-1} \text{K}^{-1}$] | $1.0 \cdot 10^3$ | $1.0 \cdot 10^3$ | $1.0 \cdot 10^3$ |
| λ_r (rock heat cond) [$\text{W m}^{-1} \text{K}^{-1}$] | 1.50 | 2.00 | 2.50 |
| ρ_r (rock density) [kg m^{-3}] | $2.25 \cdot 10^3$ | $2.25 \cdot 10^3$ | $2.25 \cdot 10^3$ |

alternatives to numerical methods for the simulation of DCBHE based on Ramey's approximation. An example of a multi-segment DCBHE made of three different segments is presented and discussed.

Table 4 CBHE properties for mass flow rate 2 kg s^{-1} .

| Segment number [-] | 1 | 2 | 3 |
|--|---------------------------------------|----------------------|----------------------|
| \dot{m} (mass flow rate) [kg s^{-1}] | 2.00 | 2.00 | 2.00 |
| A_d (area annulus) [m^2] | 0.13 | $7.23 \cdot 10^{-2}$ | $2.83 \cdot 10^{-2}$ |
| A_u (area inner tube) [m^2] | $7.85 \cdot 10^{-3}$ | $7.85 \cdot 10^{-3}$ | $7.85 \cdot 10^{-3}$ |
| v_d (velocity annulus) [m s^{-1}] | $1.52 \cdot 10^{-2}$ | $2.77 \cdot 10^{-2}$ | $7.07 \cdot 10^{-2}$ |
| v_u (velocity inner tube) [m s^{-1}] | 0.25 | 0.25 | 0.25 |
| Re_d (annulus) [-] | $4.55 \cdot 10^3$ | $5.54 \cdot 10^3$ | $7.07 \cdot 10^3$ |
| Re_u (inner tube) [-] | $2.55 \cdot 10^4$ | $2.55 \cdot 10^4$ | $2.55 \cdot 10^4$ |
| Nu_d (annulus) [-] | 3.66 | 3.66 | 3.66 |
| Nu_u (inner tube) [-] | $1.69 \cdot 10^2$ | $1.69 \cdot 10^2$ | $1.69 \cdot 10^2$ |
| U_1 (inner tube) [$\text{W m}^{-2} \text{K}^{-1}$] | $1.01 \cdot 10^3$ | $1.01 \cdot 10^3$ | $1.01 \cdot 10^3$ |
| U_2 (annulus) [$\text{W m}^{-2} \text{K}^{-1}$] | 7.32 | $1.1 \cdot 10^1$ | $2.2 \cdot 10^1$ |
| U_3 (annulus) [$\text{W m}^{-2} \text{K}^{-1}$] | 7.32 | $1.1 \cdot 10^1$ | $2.2 \cdot 10^1$ |
| $U_w dA_w/dz$ (overall for wall) [$\text{W m}^{-1} \text{K}^{-1}$] | 0.22 | 0.23 | 0.23 |
| $U_r(t)$ (overall casing-rock) [$\text{W m}^{-2} \text{K}^{-1}$] | 1.3 | 2.0 | 3.4 |
| $U_{f(t)}$ (cooling of rock) [$\text{W m}^{-2} \text{K}^{-1}$] | 1.3 | 2.0 | 3.4 |
| The heat transfer coefficients $U_r(t)$ and $U_{f(t)}$ are at $t = 10$ years | K_r (parameter) [m^{-1}] | $2.2 \cdot 10^{-4}$ | $2.6 \cdot 10^{-4}$ |
| | K_w (parameter) [m^{-1}] | $2.8 \cdot 10^{-5}$ | $2.9 \cdot 10^{-5}$ |

Acknowledgements This work is partly supported by Institute for Energy Technology, Kjeller, Norway.

Funding Open access funding provided by Institute for Energy Technology This work is partly funded by the Institute for Energy Technology, Norway.

Declarations

Conflict of interest The author states that there is no conflict of interest with the manuscript.

Appendix A: Derivation of equations and energy conservation

Conservation of energy gives a system of two Eqs. (1) and (2) for the temperature in the coaxial borehole heat exchanger. Energy conservation in a small interval of the annulus between z and $z + \Delta z$ gives

$$\begin{aligned}
 C_f \dot{m} T_d(z + \Delta z) &= C_f \dot{m} T_d(z) + U_w \Delta A_w (T_u - T_d) + 2\pi r_3 \Delta z U_r (T_r - T_d) \tag{15}
 \end{aligned}$$

where the z -axis is pointing downwards. The left-hand side is the power flowing out of the interval at $z + \Delta z$. The right-hand side is the power that flows

into the interval at z plus the power from thermal leakage of the inner tube added to the power from the surrounding rock. Similarly, the energy conservation in an interval of the inner tube between $z + \Delta z$ and z is

$$C_f \dot{m} T_u(z) = C_f \dot{m} T_u(z + \Delta z) - U_w \Delta A_w (T_u - T_d) \tag{16}$$

where the left-hand side is the power that flows out of the interval at z . The right-hand side is the power that flows into the interval at $z + \Delta x$ minus the power that leaks from the inner tube to the annulus. Recall that the flow directions are opposite in the inner tube and the annulus. The expressions for energy conservations (15) and (16) lead to Eqs. (1) and (2), respectively, in the limit $\Delta z \rightarrow 0$.

The temperature Eqs. (2) and (1) for the borehole heat exchanger can be subtracted and then integrated from $z = 0$ to $z = L$, which gives the total power produced

$$\begin{aligned}
 P_{total} &= C_f \dot{m} \cdot (T_u(0) - T_d(0)) \\
 &= 2\pi r_3 U_r(t) \int_0^L (T_r(z) - T_d(z)) dz \tag{17}
 \end{aligned}$$

when the temperature is the same at the base of the annulus and the inner tube, $T_u(L) = T_d(L)$. In the

same way, the temperature Eq. (2) for T_u can be integrated from 0 to L , and it gives the power leaked from the inner pipe to the annulus as

$$P_{leak} = C_f \dot{m} \cdot (T_u(L) - T_u(0)) = U_w \frac{dA_w}{dz} \int_0^L (T_u(z) - T_d(z)) dz. \tag{18}$$

The heat transfer coefficients do not depend on z and are taken outside the integration.

Appendix B: The temperature solution for one well segment

The coupled system of Eqs. (1) and (2) can be expressed as

$$\frac{dT}{dz} + A T = b \tag{19}$$

where the vector $T = [T_d, T_u]^T$, the matrix A is

$$A = \begin{bmatrix} (K_w + K_r(t)) & -K_w \\ K_w & -K_w \end{bmatrix} \tag{20}$$

and the vector $b = [K_r(t) T_r(z), 0]^T$. Following (Kreyszig 2020), the solution of Eq. (19) can be written as

$$\begin{bmatrix} T_d \\ T_u \end{bmatrix} = f_1(z) \begin{bmatrix} 1 \\ v_0 \end{bmatrix} + f_2(z) \begin{bmatrix} v_0 \\ 1 \end{bmatrix}, \tag{21}$$

where the functions $f_i(z)$ are expressed as

$$f_i(z) = c_i \left(az - \frac{a}{\lambda_i} + b \right) + D_i \exp(-\lambda_i z). \tag{22}$$

The vectors $v_1 = [1, v_0]^T$ and $v_2 = [v_0, 1]^T$ are eigenvectors of A , and λ_1 and λ_2 are the corresponding eigenvalues, where

$$v_0 = \frac{1}{K_w} \left(K_w + \frac{1}{2} K_r + \frac{1}{2} \sqrt{K_D} \right) \tag{23}$$

$$\lambda_{1,2} = \frac{1}{2} \left(K_r \mp \sqrt{K_D} \right), \tag{24}$$

and where $K_D = K_r^2 + 4K_w K_r$. The two constants D_1 and D_2 are determined by the boundary conditions that $T_d(z=0) = T_0$ and $T_d(z=L) = T_u(z=L)$, where L is the length of the well. The first condition is the given temperature at the inlet, and the second condition says that the temperature at the base of the well is the same in the annulus and the inner tube. The coefficients D_1 and D_2 become

$$D_1 = \frac{H_1 \exp(-\lambda_2 L) + v_0 H_2}{v_0 \exp(-\lambda_1 L) - \exp(-\lambda_2 L)} \tag{25}$$

$$D_2 = \frac{H_1 \exp(-\lambda_1 L) - H_2}{v_0 \exp(-\lambda_1 L) - \exp(-\lambda_2 L)}. \tag{26}$$

where

$$H_1 = T_0 + c_1 \left(\frac{a}{\lambda_1} - b \right) + v_0 c_2 \left(\frac{a}{\lambda_2} - b \right) \tag{27}$$

$$H_2 = -c_1 \left(aL - \frac{a}{\lambda_1} + b \right) + c_2 \left(aL - \frac{a}{\lambda_2} + b \right) \tag{28}$$

The two coefficients c_1 and c_2 are

$$c_1 = \frac{K_r}{(1 - v_0^2)\lambda_1} \quad \text{and} \quad c_2 = \frac{v_0 K_r}{(1 - v_0^2)\lambda_2}. \tag{29}$$

Appendix C: The Ramey solution

It is straightforward to show that the temperature solution (21) for the coaxial borehole heat exchanger becomes the Ramey solution (Ramey 1962) for the limit where the insulation goes to zero, which implies that $K_w \rightarrow 0$. In this limit, the eigenvalues approach $\lambda_1 \rightarrow -K_w$ and $\lambda_2 \rightarrow K_r$. Furthermore, $c_1 \rightarrow 0$ and $v_0 c_2 \rightarrow 1$, and the temperature in the annulus becomes

$$T_d(z) \approx az - aA + b + (T_0 + aA - b) \exp(-z/A) \tag{30}$$

which is Ramey’s solution (Ramey 1962), where $A = 1/\lambda_2$.

- and production. *J Petrol Sci Eng* 177:909–920. <https://doi.org/10.1016/j.petrol.2019.02.013>
- Antelmi M, Renoldi F et al (2020) Analytical and numerical methods for a preliminary assessment of the remediation time of pump and treat systems. *Water* 12(10):1–25. <https://doi.org/10.3390/w12102850>
- Bandos TV, Montero Álvaro, Fernández E et al (2009) Finite line-source model for borehole heat exchangers: effect of vertical temperature variations. *Geothermics* 38(2):263–270. <https://doi.org/10.1016/j.geothermics.2009.01.003>
- Beier RA (2011) Vertical temperature profile in ground heat exchanger during in-situ test. *Renew Energy* 36(5):1578–1587. <https://doi.org/10.1016/j.renene.2010.10.025>
- Beier RA (2020) Thermal response tests on deep borehole heat exchangers with geothermal gradient. *Appl Therm Eng* 178(115):447. <https://doi.org/10.1016/j.applthermaleng.2020.115447>
- Beier RA, Acuña J, Mogensen P et al (2013) Borehole resistance and vertical temperature profiles in coaxial borehole heat exchangers. *Appl Energy* 102:665–675. <https://doi.org/10.1016/j.apenergy.2012.08.007>
- Beier RA, Acuña J, Mogensen P et al (2014) Transient heat transfer in a coaxial borehole heat exchanger. *Geothermics* 51:470–482. <https://doi.org/10.1016/j.geothermics.2014.02.006>
- Breede K, Dzebisashvili K, Falcone G (2015) Overcoming challenges in the classification of deep geothermal potential. *Geotherm Energy Sci* 3(1):19–39. <https://doi.org/10.5194/gtes-3-19-2015>
- Bryant E (1997) *Climate process and change*. Cambridge University Press, Cambridge. <https://doi.org/10.1017/CBO9781139166751>
- Carslaw H, Jaeger J (1959) *Conduction of heat in solids*. Oxford University Press, Oxford
- Damour J, Johansson D (2016). What Vacuum Insulated Tubings Or Vacuum Insulated Casings Bring To Thermal Wells. <https://doi.org/10.2118/182515-MS>
- Diao N, Li Q, Fang Z (2004) Heat transfer in ground heat exchangers with groundwater advection. *Int J Therm Sci* 43(12):1203–1211. <https://doi.org/10.1016/j.ijthermalsci.2004.04.009>
- Diersch HJG (2013) FEFLOW: finite element modeling of flow, mass and heat transport in porous and fractured media. Springer, Berlin. <https://doi.org/10.1007/978-3-642-38739-5>
- Gascuel VL, Raymond J, Rivard C et al (2022) Design and optimization of deep coaxial borehole heat exchangers for cold sedimentary basins. SSRN, pp 1–55. <https://doi.org/10.2139/ssrn.4031127>
- Gehlin S, Spittler J, Hellström G (2016) Deep boreholes for ground-source heat pump systems—scandinavian experience and future prospects. ASHRAE Winter Conference, January 23–27, Orlando, Florida, pp 1–8
- Gola G, Di Sipio E, Facci M et al (2022) Geothermal deep closed-loop heat exchangers: a novel technical potential evaluation to answer the power and heat demands. *Renew Energy* 198:1193–1209. <https://doi.org/10.1016/j.renene.2022.08.071>
- Incorpera F, DeWitt D, Bergman T et al (2011) *Fundamentals of heat and mass transfer*, 6th edn. Wiley, New Jersey
- Ingersoll LR, Zobel OJ, Ingersoll AC (1954) *Heat Conduction with Engineering, Geological and Other Applications*. McGraw-Hill, Connaught Circus
- International Energy Agency (2016) *Energy snapshot, Global energy-related carbon dioxide emissions 1980–2016*. <https://www.iea.org/newsroom/energysnapshots>
- Kabir CS, Hasan AR, Kouba GE et al (1996) Determining circulating fluid temperature in drilling, workover, and well control operations. *SPE Drill Complet* 11:74–79
- Kohl T, Brenni R, Eugster W (2002) System performance of a deep borehole heat exchanger. *Geothermics* 31(6):687–708. [https://doi.org/10.1016/S0375-6505\(02\)00031-7](https://doi.org/10.1016/S0375-6505(02)00031-7)
- Kreyszig E (2020) *Advanced engineering mathematics*, 10th edn. Wiley, New Jersey
- Li M, Lai AC (2015) Review of analytical models for heat transfer by vertical ground heat exchangers (GHEs): a perspective of time and space scales. *Appl Energy* 151:178–191. <https://doi.org/10.1016/j.apenergy.2015.04.070>
- Luo Y, Guo H, Meggers F et al (2019) Deep coaxial borehole heat exchanger: analytical modeling and thermal analysis. *Energy* 185:1298–1313. <https://doi.org/10.1016/j.energy.2019.05.228>
- Ma L, Zhao Y, Yin H et al (2020) A coupled heat transfer model of medium-depth downhole coaxial heat exchanger based on the piecewise analytical solution. *Energy Convers Manage* 204(112):308
- Quaggiotto D, Zarrella A, Emmi G et al (2019) Simulation-based comparison between the thermal behavior of coaxial and double u-tube borehole heat exchangers. *Energies* 12(12):1. <https://doi.org/10.3390/en12122321>
- Ramey H (1962) Wellbore Heat Transmission. *J Petrol Technol* 14(04):427–435. <https://doi.org/10.2118/96-PA>
- Sanner B, Karytsas C, Mendrinou D et al (2003) Current status of ground source heat pumps and underground thermal energy storage in Europe. *Geothermics* 32(4):579–588. [https://doi.org/10.1016/S0375-6505\(03\)00060-9](https://doi.org/10.1016/S0375-6505(03)00060-9). (Selected papers from the European Geothermal Conference 2023)
- Shao H, Hein P, Sachse A et al (2016) *Geoenergy modeling II: shallow geothermal systems*. Springer, Cham. <https://doi.org/10.1007/978-3-319-45057-5>
- Sharma P, Al Saedi A, Kabir C (2020) Geothermal energy extraction with wellbore heat exchanger: analytical model and parameter evaluation to optimize heat recovery. *Renew Energy* 166:1–8. <https://doi.org/10.1016/j.renene.2020.11.116>
- Simon N, Bour O, Lavenant N et al (2021) Numerical and experimental validation of the applicability of active-dts experiments to estimate thermal conductivity and groundwater flux in porous media. *Water Resources Res* 57(1):e2020WR028078. <https://doi.org/10.1029/2020WR028078>
- Smith G (1986) Numerical solution of partial differential equations finite difference methods. *Applied Mathematics and*

- Computing Science Series. Oxford University Press, New York
- Sutton MG, Nutter DW, Couvillion RJ (2003) A ground resistance for vertical bore heat exchangers with groundwater flow. *J Energy Res Technol* 125(3):183–189. <https://doi.org/10.1115/1.1591203>
- Tóth AN, Bobok E (2008) Limits of heat extraction from dry hole. In: SGP-TR-185: Proceedings of 33rd Workshop on Geothermal Reservoir Engineering. Stanford University, Stanford University, Stanford, California, pp 1–7. <https://pangea.stanford.edu/ERE/pdf/IGAstandard/SGW/2008/toth.pdf>
- Tóth AN, Bobok E (2016) Flow and heat transfer in geothermal systems—basic equations for describing and modeling geothermal phenomena and technologies. Elsevier, Amsterdam
- Witte HJ (2007) Advances in geothermal response testing. In: Paksoy HÖ (ed) Thermal energy storage for sustainable energy consumption. Springer, Dordrecht, pp 177–192
- Zanchini E, Lazzari S, Priarone A (2010) Improving the thermal performance of coaxial borehole heat exchangers. *Energy* 35(2):657–666. <https://doi.org/10.1016/j.energy.2009.10.038>
- Zhang L, Zhang Q, Huang G (2016) A transient quasi-3d entire time scale line source model for the fluid and ground temperature prediction of vertical ground heat exchangers (GHEs). *Appl Energy* 170:65–75. <https://doi.org/10.1016/j.apenergy.2016.02.099>

Publisher's Note Springer Nature remains neutral with regard to jurisdictional claims in published maps and institutional affiliations.